



HAL
open science

The LXCXE Retinoblastoma Protein-Binding Motif of FOG-2 Regulates Adipogenesis

O Goupille, T Penglong, Z Kadri, M Granger-Locatelli, R Denis, S Luquet, C Badoual, S Fucharoen, L Maouche-Chretien, P Leboulch, et al.

► **To cite this version:**

O Goupille, T Penglong, Z Kadri, M Granger-Locatelli, R Denis, et al.. The LXCXE Retinoblastoma Protein-Binding Motif of FOG-2 Regulates Adipogenesis. *Cell Reports*, 2017, 21 (12), pp.3524-3535. 10.1016/j.celrep.2017.11.098 . hal-03108274

HAL Id: hal-03108274

<https://cnrs.hal.science/hal-03108274v1>

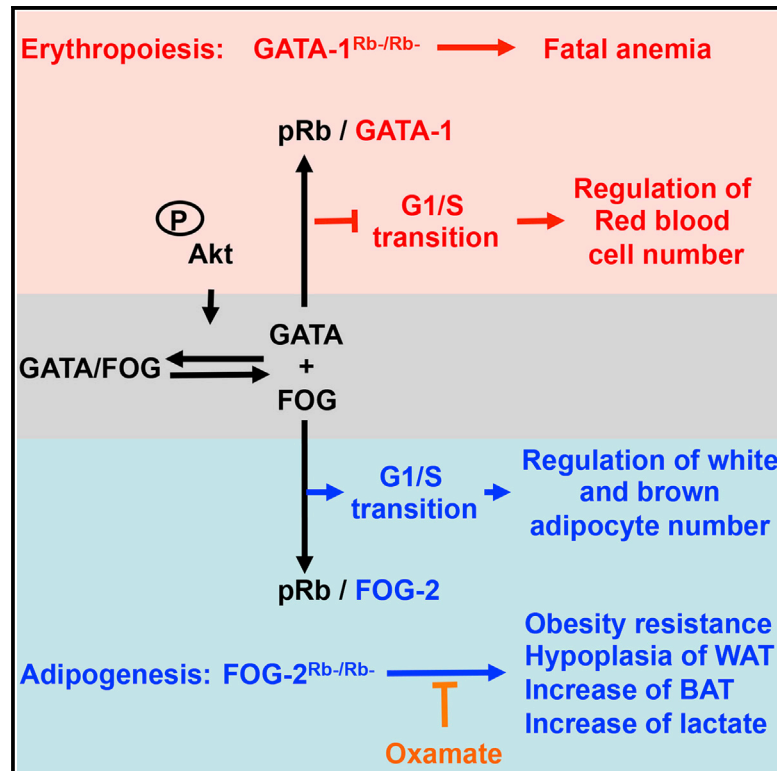
Submitted on 15 Nov 2022

HAL is a multi-disciplinary open access archive for the deposit and dissemination of scientific research documents, whether they are published or not. The documents may come from teaching and research institutions in France or abroad, or from public or private research centers.

L'archive ouverte pluridisciplinaire **HAL**, est destinée au dépôt et à la diffusion de documents scientifiques de niveau recherche, publiés ou non, émanant des établissements d'enseignement et de recherche français ou étrangers, des laboratoires publics ou privés.

The LXCXE Retinoblastoma Protein-Binding Motif of FOG-2 Regulates Adipogenesis

Graphical Abstract



Authors

Olivier Goupille, Tipparat Penglong, Zahra Kadri, ..., Leila Maouche-Chrétien, Philippe Leboulch, Stany Chrétien

Correspondence

stany.chretien@cea.fr

In Brief

Goupille et al. find that a mutation of the FOG-2 LXCXE pRb-binding site decreases cell proliferation and affects adipogenesis *in vitro* and *in vivo*. $Fog2^{Rb-/Rb-}$ mutant mice are resistant to obesity, and they present abnormal WAT/BAT conversion and lactate production. Oxamate treatment results in phenotype reversion in these mice.

Highlights

- $FOG-2^{Rb-}$ expression slows down G1/S cycle transition and reduces cell proliferation
- The LXCXE pRb-binding site of FOG-2 ($FOG-2^{Rb-}$) is involved in adipogenesis
- $Fog2^{Rb-/Rb-}$ mice are resistant to obesity and present abnormal WAT/BAT conversion
- Oxamate reverses the adiposity of WT and $Fog2^{Rb-/Rb-}$ mice *in vitro* and *in vivo*

Data and Software Availability

GSE90859



The LXCXE Retinoblastoma Protein-Binding Motif of FOG-2 Regulates Adipogenesis

Olivier Goupille,¹ Tipparat Penglong,^{1,2} Zahra Kadri,¹ Marine Granger-Locatelli,¹ Raphaël Denis,³ Serge Luquet,³ Cécile Badoual,⁴ Suthat Fucharoen,² Leila Maoche-Chrétien,^{1,5} Philippe Leboulch,^{1,2,6} and Stany Chrétien^{1,5,7,*}

¹Service des Thérapies Innovantes, Institute Jacob, CEA 92265 Fontenay-aux-Roses and University Paris Saclay UMR-E007, 91405 Orsay Cedex, France

²Thalassemia Research Center, Institute of Molecular Biosciences, Mahidol University, 73170 Nakhon Pathom, Thailand

³Unité de Biologie Fonctionnelle et Adaptative, Centre National la Recherche scientifique, UMR 8251, Université Paris Diderot, Sorbonne Paris Cité, 75205 Paris, France

⁴Department of Pathology, G. Pompidou European Hospital APHP-Université Paris Descartes, Paris, France

⁵INSERM, Paris, France

⁶Genetics Division, Department of Medicine, Brigham and Women's Hospital and Harvard Medical School, Boston, MA 02215, USA

⁷Lead Contact

*Correspondence: stany.chretien@cea.fr
<https://doi.org/10.1016/j.celrep.2017.11.098>

SUMMARY

GATA transcription factors and their FOG cofactors play a key role in tissue-specific development and differentiation, from worms to humans. Mammals have six GATA and two FOG factors. We recently demonstrated that interactions between retinoblastoma protein (pRb) and GATA-1 are crucial for erythroid proliferation and differentiation. We show here that the LXCXE pRb-binding site of FOG-2 is involved in adipogenesis. Unlike GATA-1, which inhibits cell division, FOG-2 promotes proliferation. Mice with a knockin of a *Fog2* gene bearing a mutated LXCXE pRb-binding site are resistant to obesity and display higher rates of white-to-brown fat conversion. Thus, each component of the GATA/FOG complex (GATA-1 and FOG-2) is involved in pRb/E2F regulation, but these molecules have markedly different roles in the control of tissue homeostasis.

INTRODUCTION

The members of the GATA family of transcription factors (six members in mammals) have a highly conserved zinc-finger DNA-binding domain that specifically binds a consensus DNA sequence (A/T)GATA(A/G). The functions of GATA proteins are regulated by cofactors, such as Friend of GATA (FOG). These cofactors bind exclusively to the N-terminal zinc finger of GATA protein, are unable to bind DNA, have no independent function, and act together with GATA to control cell differentiation (Chlon and Crispino, 2012).

The FOG family contains only two members: FOG-1 and FOG-2. GATA-1/2/3 and FOG-1 are predominantly expressed in hematopoietic cells, whereas the other GATA members and FOG-2 participate in control of the differentiation of most other cell types (Cantor and Orkin, 2005; Patient and McGhee, 2002). The roles of GATA-1/FOG-1 complexes in red blood cell production are well established, and both factors are involved in regulating the

expression of many erythroid genes (Cantor and Orkin, 2002). A role for GATA-1 in the arrest of cell proliferation has been described (Rylski et al., 2003; Kadri et al., 2005; Zhao et al., 2006). Our recent discovery of an LXCXE pRb-binding site (Morris and Dyson, 2001) at Nter of GATA-1, which is involved in the direct association of GATA-1 with the retinoblastoma protein (pRb), provides a molecular explanation for this function (Kadri et al., 2015): sequestration of E2F2 by the GATA-1/pRb complex results in cell cycle break at the G1/S transition, a crucial step for erythroid maturation (Kadri et al., 2009). The resumption of normal cell cycle kinetics is induced by erythropoietin, which triggers the phosphorylation of GATA-1 at Ser³¹⁰ by AKT, thereby increasing the affinity of GATA-1 for FOG-1 (Kadri et al., 2015). In turn, FOG-1 displaces pRb/E2F2 from phosphorylated GATA-1, ultimately releasing free, pro-proliferative E2F2. Mice bearing a *Gata1*^{S370A} mutation suffer from fatal anemia when a compensatory pathway for E2F2 production involving IGF-I signaling is simultaneously abolished (Kadri et al., 2015). Thus, GATA-1, FOG-1, pRb, E2F2, erythropoietin, and IGF-I are involved in coordinating expansion/maturation during red blood cell production (Figure 1).

Surprisingly, the few studies that have been published suggest that the other GATA factors have no direct function on cell proliferation (Chlon and Crispino, 2012; Tsai et al., 2005; Zeisberg et al., 2005), contrasting strongly with the inhibitory effect of GATA-1 on cell proliferation (Kadri et al., 2005; Rylski et al., 2003). The disruption of GATA or pRb protein production results in convergent phenotypes. Knockouts of *Gata2* and *Gata3* are associated with obesity (Jack and Crossley, 2010; Tong et al., 2000), and FOG-2 overproduction interferes with adipogenesis (Jack and Crossley, 2010; Tong et al., 2000), whereas *E2f1*^{-/-} (Blanchet et al., 2011; Aguilar and Fajas, 2010) and *pRb*^{-/-} mice (Calo et al., 2010; Dali-Youcef et al., 2007; Hansen et al., 2004; Mercader et al., 2009) are resistant to diet-induced obesity and develop a marked thermogenic phenotype. The Hedgehog-mediated inhibition of adipogenesis requires GATA-2 or -3 expression (Suh et al., 2006), and GATA/COUP-TFII interaction has antiadipogenic effects (Xu et al., 2008). Decreases in GATA-2 expression promote brown adipogenesis (Tsai et al., 2005), and conditional pRb knockout (KO) regulates white/brown adipocyte conversion or fate choice (Aguilar and Fajas, 2010).



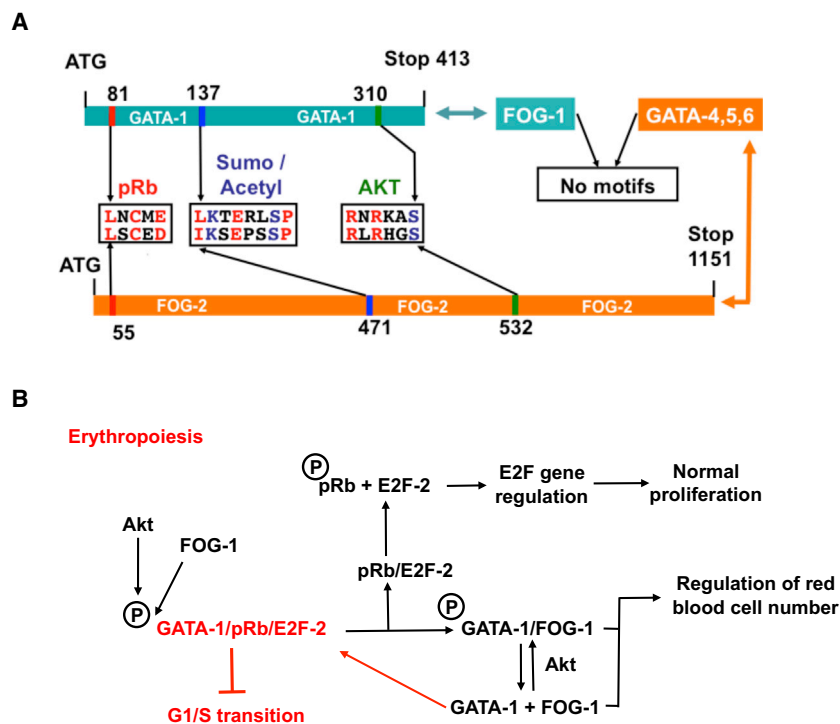


Figure 1. Only GATA-1 and FOG-2 Proteins Share Common Peptidic Sequences

(A) Amino acid sequence comparison of GATA-1 and FOG-2. Nter LXCXE motif that can bind to pRb is indicated. See also Figure S1A.

(B) Schematic model of the coordination of cell proliferation and maturation during erythropoiesis (Kadri et al., 2015).

etic GATA proteins (Tevosian et al., 1999; Patient and McGhee, 2002), contains a potential pRb-binding sequence at position 55 in the N terminus of the protein as well as a Ser residue, a potential target for AKT phosphorylation, at position 532 (Figure 1A; Figure S1A). We also identified another consensus sequence (LKXEXXSP), at position 137 in GATA-1 and 471 in FOG-2, in which the lysine may be either sumoylated or acetylated depending on the phosphorylation state of the Ser residue (Shalizi et al., 2006) (Figure 1A; Figure S1A). As FOG-2 and GATA-1 are not phylogenetically related, the presence of these three conserved sequences in the same configuration is statistically implausible. Based on our published results for

This cell-autonomous function of pRb, increasing the capacity for brown-like adipogenesis, was confirmed in recent studies (Hu et al., 2015; Petrov et al., 2016). Altogether, GATA, pRb, and E2F1 are intrinsically involved in adipogenesis.

In this study, we provide potential molecular explanations for these observations. We show that, like GATA-1 (Kadri et al., 2009), the LXCXE pRb-binding site of FOG-2 is involved in adipogenesis. Unlike GATA-1, which inhibits cell division, FOG-2 stimulates proliferation. In both cases, mutation of the LXCXE motif reverts the respective phenotypes. Knockin homozygous mice for a point mutation affecting the FOG-2 pRb-binding domain (*Fog2^{Rb-IRb-}*) are hyperactive and resistant to obesity. These mice have better adaptive thermogenesis associated with higher rates of conversion of white to brown fat, and they display an abnormal response to metabolic drugs. Thus, only GATA-1 and FOG-2 are involved in E2F regulation, with negative and positive effects, respectively, on cell proliferation.

RESULTS

Only GATA-1 and FOG-2 Proteins Have Peptide Motifs in Common

The GATA-1 amino acid sequence contains an N-terminal pRb-binding motif, LXCXE, at position 81 and a Ser residue that can be phosphorylated by AKT at position 310 (Kadri et al., 2005, 2009; Zhao et al., 2006) (Figure 1A). Mice with a mutation of the LXCXE motif of GATA-1 die from anemia at embryonic day (E)11 (Kadri et al., 2009). All six GATA proteins have an N-terminal activation domain, but the primary sequences of these proteins diverge considerably, and only GATA-1 contains the pRb-binding motif LXCXE. Surprisingly, FOG-2, a cofactor of non-hematopoi-

GATA-1 (Kadri et al., 2005, 2009, 2015) (see model at Figure 1B), this last finding for FOG-2 led us to investigate first the putative functions of the LXCXE sequence and to compare the results obtained for FOG-2 with those for GATA-1.

Fog2^{Rb-IRb-} Mutant Mice Are Resistant to Obesity and Present Abnormal WAT/BAT Conversion

To evaluate the physiological importance of the LXCXE pRb motif of FOG-2 *in vivo*, we mutated this sequence in a *Fog2^{Rb-}* knockin (KI) mouse strategy (Figures S1B and S2; Experimental Procedures). As expected, FOG-2 and *Fog2^{Rb-}* protein expression was similar in heart, muscle, brain, and adipose tissues. Of note, FOG-2 expression was low in abdominal white adipose tissue (WAT) and in liver (Figure S2D). Homozygote KI mice expressing the mutant *Fog2^{Rb-}* allele developed normally, but they were resistant to age-associated obesity independently of sex (Figures S3A and S3B). The macroscopic appearance of *Fog2^{Rb-IRb-}* livers indicated resistance to hepatosteatosis, and *Fog2^{Rb-IRb-}* mice were hyperactive (Figures S3C and S3D). H&E staining of inguinal and scapular WAT revealed that aged *Fog2^{Rb-IRb-}* mice present adipocyte hypotrophy associated with abnormally large numbers and sizes of mitochondria (Figures S3E–S3H). *Fog2^{Rb-IRb-}* inguinal WAT revealed smaller adipocytes and cells with a specific morphology, suggesting a phenotypic transition to brown adipose tissue (BAT) (Figure S3E). *Fog2^{Rb-IRb-}* scapular WAT contained smaller lipid droplets (Figure S3E).

To confirm these observations, 12-week-old mice were fed low-fat or high-fat diets for 6 weeks. Wild-type (WT) mice under high-fat diet became obese, whereas *Fog2^{Rb-IRb-}* mice kept a lean phenotype (Figure 2; Figure S4). *Fog2^{Rb-IRb-}* WAT abdominal adipocytes were larger than those in control mice but were

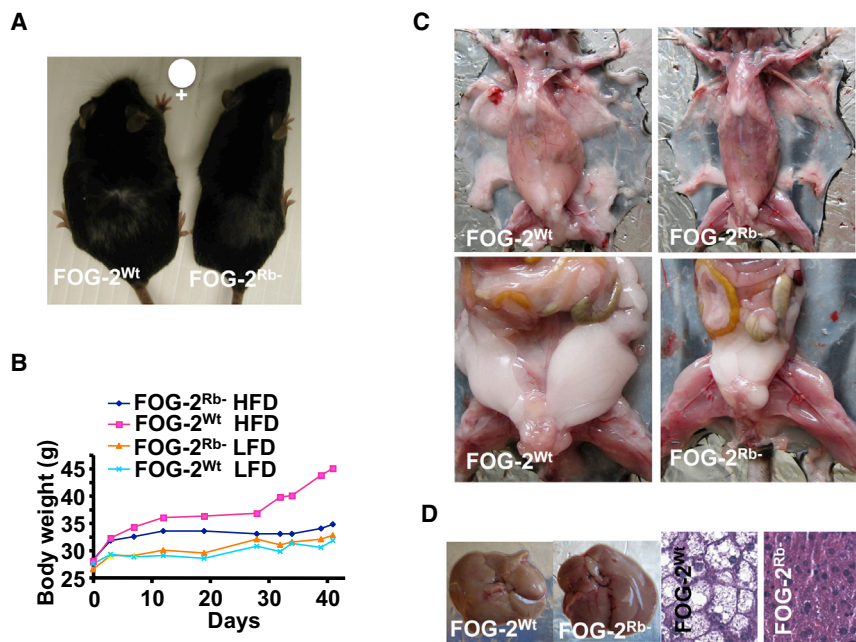


Figure 2. FOG-2^{Rb-/-} Expression Prevents Weight Gain in Mice Fed a High-Fat Diet

(A) Comparison of WT and *Fog2*^{Rb-/-} female mice (8 weeks old, n = 6 per group) fed a 45% high-fat diet (HFD) for 6 weeks (Δ BW = 11.11 \pm 3.51 g). See also Figure S4. (B) Mean body weight gain of WT and *Fog2*^{Rb-/-} female mice fed a low-fat diet (LFD) or a HFD for 6 weeks (n = 6 per group). (C) Macroscopic comparison of subcutaneous and abdominal fat. (D) Macroscopic comparison of livers and H&E staining of liver sections.

less numerous (hypoplasia) (Figure 3A). A lower recruitment of new adipocytes from preadipocytes or a preexisting adipocyte hypoplasia in *Fog2*^{Rb-/-Rb-/-} mice could explain this phenotype. H&E staining of *Fog2*^{Rb-/-Rb-/-} inguinal WAT (low-fat diet conditions; Figure 3A) or *Fog2*^{Rb-/-Rb-/-} peritoneal fat (Figure 3C) revealed areas characteristic of the phenotypic transition to BAT adipocytes. For both diets, scapular BAT and WAT were analyzed and found to display no marked histological differences (Figure 3B). An analysis of specific markers of the BAT, such as uncoupling protein 1 (UCP1), the mitochondrial respiratory chain (Cox5a), fatty acid oxidation (Cpt1b) (Figure 3D), and the number and size of mitochondria (Figure 3E; Figure S3H) indicated that mutation of the LXCXE pRb-binding site of FOG-2 might increase generation of the BAT phenotype in inguinal and scapular fat.

FOG-2^{Rb-/-Rb-/-} MEFs and Preadipocytes Have Abnormally Low Levels of Proliferation

To explore the intrinsic consequence of the FOG-2 mutation on adipogenesis, we generated mouse embryonic fibroblasts (MEFs) from these mice: *Fog2*^{Rb-/-Rb-/-} MEFs proliferated less strongly than WT MEFs (Figure 4A). The cell cycle profiles of asynchronously growing MEFs showed a significantly higher proportion of cells in the G1 phase for *Fog2*^{Rb-/-Rb-/-} MEFs (Figure 4B). Compared to WT MEFs, *Fog2*^{Rb-/-Rb-/-} MEFs differentiated less (Figure 4C). To confirm the involvement of the FOG-2 LXCXE motif in cell proliferation, we determined gene expression profiles by microarray analysis (Experimental Procedures). This analysis was conducted with RNA samples prepared from *Fog2*^{Rb-/-Rb-/-} MEFs and WT MEFs on day -4 (Figure 4A; 1 day before the significant decrease in *Fog2*^{Rb-/-Rb-/-} MEF proliferation) to prevent bias in the results and to ensure that only genes displaying early differential expression would be identified. We found that the expression of 1,587 genes was significantly modified, by a factor of more than 1.3, by FOG-2^{Rb-/-} expression (p < 0.01).

As expected, ingenuity pathway analysis identified supernetworks in which most of the targeted genes were involved in cell proliferation (p = 1.43 \times 10⁻²⁷) and cell cycle progression (p = 3.07 \times 10⁻¹³; Figure 4D). Previous observations, hypotheses, and this last analysis confirmed the importance of FOG-2/pRb association in the control of proliferation. The heatmap for misregulated genes confirmed our hypothesis and the lists of genes directly involved in cell proliferation, expression of genes under *E2f1* control, or both these processes are indicated in Figures 4E-4G. In particular, *Pdk4* expression, which was stronger in *E2f1*^{-/-} BAT (Blanchet et al., 2011) and *Fog2*^{Rb-/-Rb-/-} BAT (Figures 3D, 6D, and 6E), was also stronger in proliferating *Fog2*^{Rb-/-Rb-/-} MEFs (Figure 4F). The regulation of *Mcm5*, *Mcm6* (Ohtani et al., 1999), and *Psat1* (Yang et al., 2015) expression and the functions of the products of these genes as activators during progression through the G1/S phase of the cell cycle are consistent with our results (Figure 4B versus Figures 4F and 4G). The higher levels of *Cyb5a* (Giovannetti et al., 2014) or *Eya4* (Mo et al., 2016) tumor suppressor expression may also account for the proliferation defect seen in *Fog2*^{Rb-/-Rb-/-} MEFs (Figure 4G). Overall, our analysis suggests that the mutation of the FOG-2 binding to pRb is sufficient to disturb proliferation and cell cycle control, with E2F as an upstream regulator.

To confirm the potential intrinsic role of the FOG-2 on cell proliferation, we turned to primary culture of preadipocyte cells that are able to differentiate in adipocyte. We generated mouse preadipocytes from inguinal WAT of *Fog2*^{WT} and of *Fog2*^{Rb-/-Rb-/-} mice: *Fog2*^{Rb-/-Rb-/-} preadipocytes proliferated less strongly than WT preadipocytes (Figure 4H). Compared to WT preadipocytes, *Fog2*^{Rb-/-Rb-/-} preadipocytes differentiated less (Figures 4I and 4J). Altogether, the lower proliferation capacity of *Fog2*^{Rb-/-Rb-/-} MEFs (Figures 4A-4G) and *Fog2*^{Rb-/-} preadipocyte cells (Figures 4H-4J) is consistent with an adipocyte hypoplasia shown in Figure 3A.

To confirm the potential intrinsic role of the FOG-2 on cell proliferation, we turned to primary culture of preadipocyte cells that are able to differentiate in adipocyte. We generated mouse preadipocytes from inguinal WAT of *Fog2*^{WT} and of *Fog2*^{Rb-/-Rb-/-} mice: *Fog2*^{Rb-/-Rb-/-} preadipocytes proliferated less strongly than WT preadipocytes (Figure 4H). Compared to WT preadipocytes, *Fog2*^{Rb-/-Rb-/-} preadipocytes differentiated less (Figures 4I and 4J). Altogether, the lower proliferation capacity of *Fog2*^{Rb-/-Rb-/-} MEFs (Figures 4A-4G) and *Fog2*^{Rb-/-} preadipocyte cells (Figures 4H-4J) is consistent with an adipocyte hypoplasia shown in Figure 3A.

FOG-2^{Rb-/-Rb-/-} Mutant Mice, MEFs, and Preadipocytes Present Abnormal WAT/BAT Shift, and FOG-2^{Rb-/-Rb-/-} Mutant Mice Are Resistant to Cold Stress

We went back to our MEF and preadipocytes models to confirm the potential WAT/BAT conversion of *Fog2*^{Rb-/-Rb-/-} inguinal WAT (low-fat diet conditions; Figure 3A) or *Fog2*^{Rb-/-Rb-/-} peritoneal fat

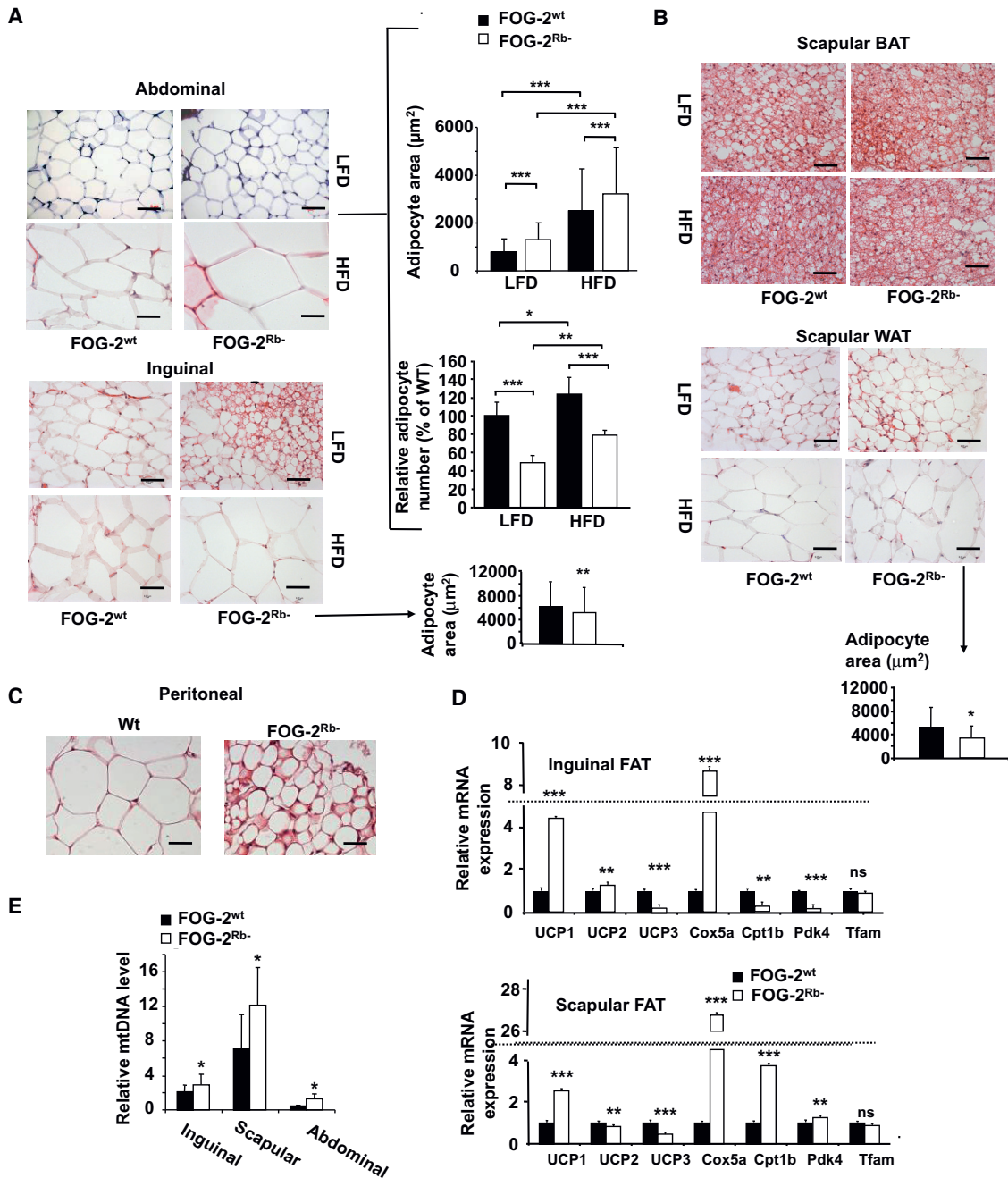


Figure 3. *Fog2^{Rb-/Rb-}* Mutant Mice Present Adipocyte Hypotrophy Associated with Abnormal WAT/BAT Conversion

(A–C) Representative H&E staining sections of abdominal FAT (A), inguinal FAT (A), scapular BAT (B), scapular WAT (B), and peritoneal (C) from 12-week-old WT and *Fog2^{Rb-/Rb-}* male mice fed a LFD or a HFD (6 weeks; scale bar, 50 μm ; and $n = 6$ per group). The cell surface average (μm^2) was estimated by measurement on histological sections, and the weight of each tissue was used to evaluate the relative adipocyte numbers (% of WT under LFD) in abdominal FAT (one-way ANOVA with Bonferroni post-test, $\alpha = 0.05$).

(D) Relative expression by qRT-PCR of relevant BAT or mitochondrial genes involved in oxidative metabolism and thermogenesis in inguinal and scapular FAT of 12-week-old WT and *Fog2^{Rb-/Rb-}* male mice (Student's t test, $n = 3$ /genotype).

(E) mtDNA qPCR estimation of the mitochondrial number in the different FAT pads (Student's t test, $n = 3$ /genotype). See also Figure S3H.

Data are mean \pm SD.

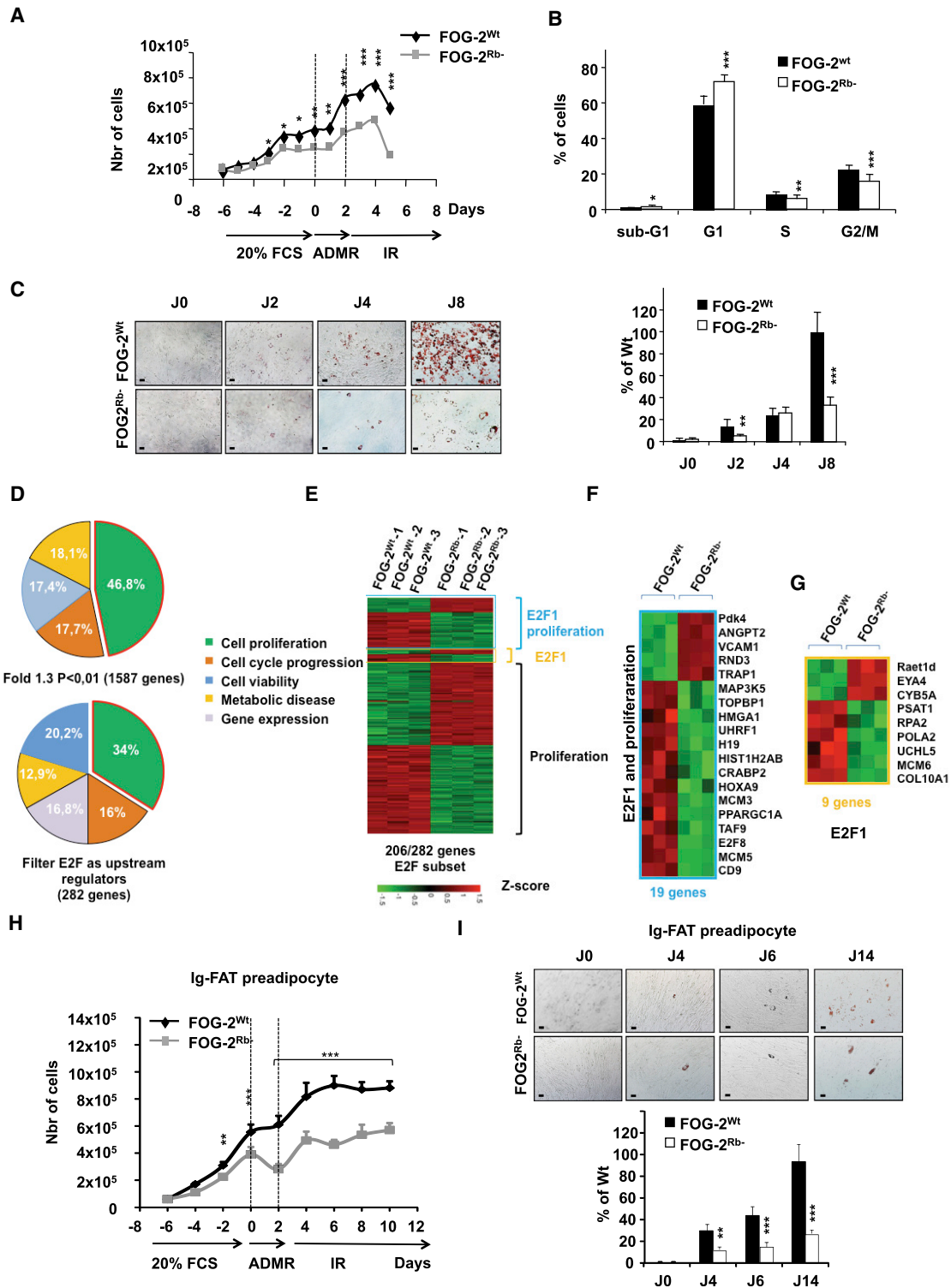


Figure 4. *Fog2*^{Rb-/-Rb-} MEFs and Preadipocytes Have Abnormally Low Levels of Proliferation, and FOG-2 Regulates the Expression of E2F-Regulated Genes

(A) Comparison of the timescale of WT and *Fog2*^{Rb-/-Rb-} E14.5 MEF proliferation before and after the onset of differentiation (J0) by two-way ANOVA with Bonferroni post-test ($\alpha = 0.05$, $n = 3$).

(B) Cell cycle profile of asynchronously growing WT and *Fog2*^{Rb-/-Rb-} MEFs (Student's t test, $n = 5$).

(legend continued on next page)

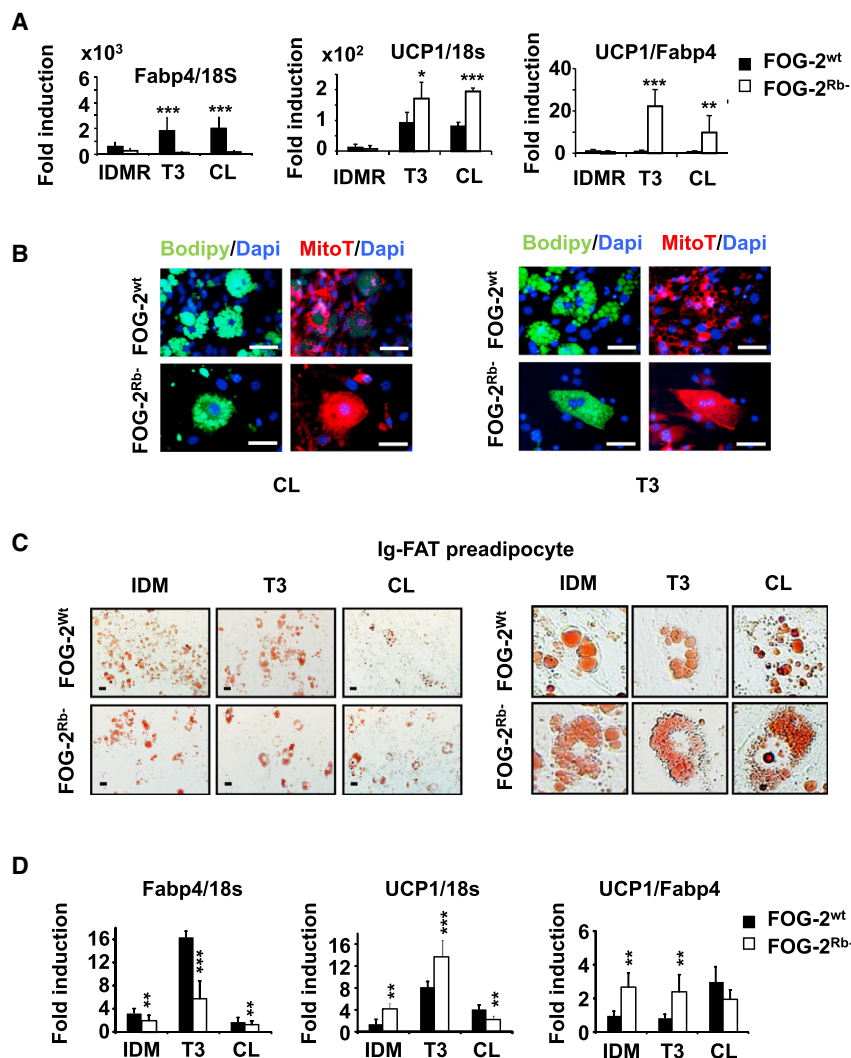


Figure 5. Differentiated *Fog2^{Rb-/Rb-}* MEFs Display the Characteristics of Brown Adipocytes

(A) qRT-PCR quantification of the relative levels of *Ucp1* (adipocyte browning) and *Fabp4* (general adipogenesis) expression of differentiated WT and *Fog2^{Rb-/Rb-}* E14.5 MEFs in the absence (IDMR) or in the presence (T3, CL). The fold change in *Ucp1* expression relative to 18 s or *Fabp4* is shown (n = 3 per treatment, one-way ANOVA t test with Bonferroni post-test (n = 3)).

(B) Lipid droplets (Bodipy 493/503), mitochondria (MitoTracker-Red), and the nuclei (Hoechst) fluorescent staining of differentiated WT and *Fog2^{Rb-/Rb-}* MEFs.

(C) Oil red staining of inguinal WT and *Fog2^{Rb-/Rb-}* preadipocytes cultivated in WAT (IDM) or BAT (T3 or CL) differentiating medium for 18 days.

(D) As in (A), same experiments were repeated in preadipocytes (n = 6 per treatment and genotype). Data are mean ± SD.

As the conversion from white to brown adipocytes is associated with adaptive thermogenesis, we challenged mice with cold. *Fog2^{Rb-/Rb-}* mice maintained body temperature longer than controls (Figure 6A) due to an increase in BAT differentiation within the inguinal WAT (Figures 3A and 6B, 30°C). After exposure to 4°C for 10 days, the conversion rate of WAT to BAT was equivalent in WT and *Fog2^{Rb-/Rb-}* mice (Figure 6B, 4°C). Moreover, electron microscopy analysis revealed features characteristic of a BAT phenotype within the *Fog2^{Rb-/Rb-}* inguinal tissue: an increase in the number and size of mitochondria and a decrease in the size of lipid droplets (Figure 6C). In a thermo-

neutral environment, expression analysis of genes differentially expressed in BAT versus WAT confirmed the presence of BAT within WAT in *Fog2^{Rb-/Rb-}*, but not in WT mice (Figures 6D and 6E). After cold exposure, an expression increase of BAT markers was observed in both mouse genotypes: BAT in *Fog2^{Rb-/Rb-}* reached a plateau and BAT in WT mice caught up with the mutant mice level after cold exposure (Figures 6D and 6E). As a control, analysis of scapular BAT indicated an equivalent enhancement of BAT markers in both cases (Figure S5D). An analysis of adiposity parameters under cold stress confirmed that *Fog2^{Rb-/Rb-}* mice were already well adapted to this stress and maintained their adiposity, whereas WT mice

(Figure 3C). When BAT differentiation was promoted by the addition of T3 and the β -adrenergic agonist CL 316,243 (CL), *Fog2^{Rb-/Rb-}* MEFs and preadipocytes developed BAT characteristics, with a consistent and significant upregulation of *Ucp1* (Figures 5A and 5D). For MEF cells, a specific distribution of intracellular lipids staining by Bodipy (small clustered lipid droplets in the brown adipocytes and unilocular droplets in the white adipocytes) and a stronger staining of mitochondria with MitoTracker Red are visualized (Figure 5B). For *Fog2^{Rb-/Rb-}* preadipocyte cells, the observed morphology resembles brown-like lipids with small lipid droplets that form clusters with multilocular appearance (Figure 5C).

neutral environment, expression analysis of genes differentially expressed in BAT versus WAT confirmed the presence of BAT within WAT in *Fog2^{Rb-/Rb-}*, but not in WT mice (Figures 6D and 6E). After cold exposure, an expression increase of BAT markers was observed in both mouse genotypes: BAT in *Fog2^{Rb-/Rb-}* reached a plateau and BAT in WT mice caught up with the mutant mice level after cold exposure (Figures 6D and 6E). As a control, analysis of scapular BAT indicated an equivalent enhancement of BAT markers in both cases (Figure S5D). An analysis of adiposity parameters under cold stress confirmed that *Fog2^{Rb-/Rb-}* mice were already well adapted to this stress and maintained their adiposity, whereas WT mice

(C) Oil red staining of WT and *Fog2^{Rb-/Rb-}* MEFs during adipogenesis (scale bar, 50 μ m) with a quantification of staining on the right (two-way ANOVA with Bonferroni post-test, $\alpha = 0.05$; n = 3).

(D) Pie charts showing the gene distribution in a classification indicating the percentage of genes belonging to specific groups, as indicated (ingenuity pathway analysis on 1,587 genes, using a threshold of 1.3 with p < 0.01).

(E–G) Heatmaps for *E2f1*-related genes (E), proliferation-related genes and *E2f1*-related genes (F), and *E2f1*-related genes (G) as indicated.

(H and I) As in (A) and (C), same experiments were repeated in preadipocyte (n = 9). Scale bar, 50 μ m.

Data are mean ± SD.

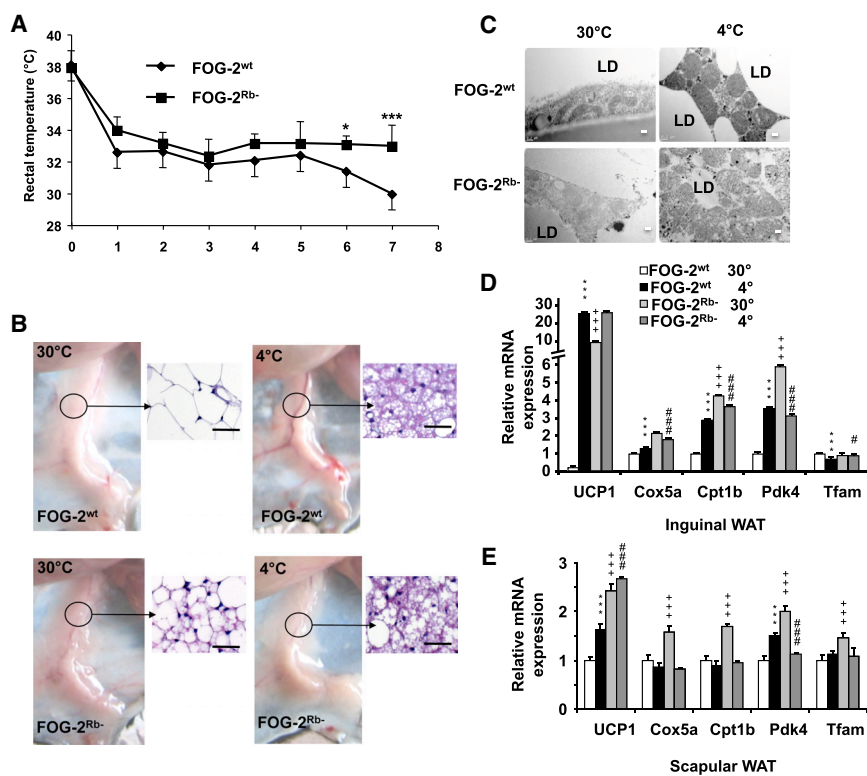


Figure 6. *Fog2^{Rb-IRb-}* Mice Are Resistant to Cold Stress

(A) Time course (hours) of rectal temperature of 10-week-old WT and *Fog2^{Rb-IRb-}* male mice exposed to a stress cold (4°C) for 7 hr (two-way ANOVA with Bonferroni post-test, $\alpha = 0.05$; $n = 4$ /genotype). (B) Macroscopic observation and H&E staining of sections of inguinal WAT from WT and *Fog2^{Rb-IRb-}* male mice at thermo-neutrality (30°C) or cold-adapted (4°C) for 10 days ($n = 5$ /genotype; scale bar, 50 μ m) under a regular diet. See also Figure S5.

(C) Representative electron micrographs of inguinal sections from (B) focused on mitochondria ($\times 40,000$; scale bar, 0.2 μ m). The localization of the lipid droplet (LD) is indicated.

(D and E) qRT-PCR relative expression of relevant genes involved in BAT and mitochondrial metabolism in inguinal (D) and scapular (E) WAT ($n = 3$ /group). *WT 30°C versus WT 4°C, #WT 30°C versus *Fog2^{Rb-IRb-}* 30°C, #WT 4°C versus *Fog2^{Rb-IRb-}* 4°C (one-way ANOVA with Bonferroni post-test, $\alpha = 0.05$). See also Figure S5D. Data are mean \pm SD.

lost weight and increased the browning of WAT (Figure 6; Figure S5).

Fasted Homozygous *Fog2^{Rb-IRb-}* Mutant Mice Have Lactic Acidosis and an Alteration of Metabolism

Serum glucose levels were slightly lower, insulin secretion lower, and serum lactate levels higher in *Fog2^{Rb-IRb-}* than WT mice (Figure S6A). This suggests that the mutation of the LXCXE pRb-binding site of FOG-2 may be involved in the anaerobic glycolytic pathway in muscle and in hepatic gluconeogenesis (Cori cycle). Glucose and insulin tolerance tests indicated that *Fog2^{Rb-IRb-}* mice were not diabetic but were apparently hypersensitive to insulin (Figure S6B). We performed lactate and pyruvate tolerance tests to determine why *Fog2^{Rb-IRb-}* mice had a higher level of lactate. These mice displayed intolerance to both lactate and pyruvate, and a lower capacity than WT to convert lactate and pyruvate to glucose (Figures S6C and S6D). Lactate metabolism in the liver plays important roles in buffering blood lactate levels. In the Cori cycle, the liver takes up lactate and converts it into pyruvate, which then serves as a substrate for gluconeogenesis.

We thus compared the mRNA levels of genes involved in key enzymes that commit pyruvate/lactate to hepatic neoglucogenesis (*G6pc*, *Pck1*, *Pcx*, and *Pklr*), that are involved in pyruvate conversion to lactate (*Ldha*), and that are engaged in metabolite transportation (*Mct1* for lactate transport and *Mpc2* for pyruvate transport). The global expression profile in the liver of *Fog2^{Rb-IRb-}* mice was altered relative to WT mice after 16 hr of fasting: *Mpc2*, *G6pc*, and *Pck1* expression levels decreased significantly (Figure S6E). In contrast, *Ldha* and

Mct1 expression levels increased. Hence, the expression profile observed in *Fog2^{Rb-IRb-}* mice is consistent with their high blood lactate concentration observed after lactate and pyruvate challenge (Figures S6C and S6D). Therefore, *Fog2^{Rb-IRb-}* mice seem to suffer from a defect in hepatic gluconeogenesis, the pathophysiology of which remains to be understood.

As Leptin promotes GATA-3 expression in the liver and controls the inhibition of PPAR γ 1 (Guan et al., 2017), we investigated the resistance to hepatosteatosis of *Fog2^{Rb-IRb-}* livers by evaluating Leptin levels in *Fog2^{Rb-IRb-}* mice. These levels were lower in the mutant mice than in WT, providing a potential explanation for the observed phenotype (Figure S6F). Resistance to hepatosteatosis in *Fog2^{Rb-IRb-}* mice may result from an indirect (Leptin production). Direct implication of GATA-3/FOG-2/pRb pathway deregulation in hepatosteatosis of *Fog2^{Rb-IRb-}* livers is possible, but the very low level of FOG-2 protein expression in liver (Figure S2D) is against this hypothesis.

Given the lack of a link between FOG-2 and total energy expenditure, we addressed this question by making extensive analyses of metabolism using indirect calorimetric analysis in a controlled environment, as described in the Supplemental Experimental Procedures. Compared to *Fog2^{Rb-IRb-}* littermate, *Fog2^{Rb-IRb-}* mice displayed a significant decrease in whole-energy expenditure (Figure S7A). The effect on energy expenditure stemmed from the decrease of the resting metabolism (Supplemental Experimental Procedures and Figure S7B). Concomitant analysis of food intake (expressed in kcal/kg lean body mass) showed a significance decrease of food intake in *Fog2^{Rb-IRb-}* mice (Figure S7C). Interestingly, energy balance calculated during the same period showed that WT animals were in significant positive energy balance compared to the *Fog2^{Rb-IRb-}* mice (Figure S7D). These differences could explain the differences in body

weight. However, the lower level of resting metabolism (Figure S7B) and an increase in lipid oxidation (Figure S7E) indicate that peripheral tissue metabolism was adapted for the preferential use of lipid substrates.

Oxamate Reverses the Adiposity of WT and *Fog2^{Rb-/-Rb-}* Mice *In Vitro* and *In Vivo*

The concentration of lactate in the blood was high in *Fog2^{Rb-/-Rb-}* mice (Figure S6A), and lactate has been identified as a WAT-browning factor (Carrière et al., 2014; Vergnes and Reue, 2014). Various metabolic processes are coupled with pRb/E2F cell cycle regulators (Aguilar and Fajas, 2010). We therefore explored the importance of this cellular metabolite in our model. We tested the effects of drugs that disturb pyruvate/lactate metabolism, including oxamate (OXA) and phenylacetate (PA), which inhibit lactate dehydrogenase (LDH) and pyruvate carboxylase (PC), respectively. Only OXA has the most significant differential effects on adipogenesis: complete restoration of *Fog2^{Rb-/-Rb-}* MEF differentiation and inhibition of WT MEF differentiation (Figure 7A). Once again, these MEF experiments support the conclusion that *Fog2^{Rb-}* defects are, at least in part, cell intrinsic.

To confirm this observation *in vivo*, WT and *Fog2^{Rb-/-Rb-}* mice were treated for 5 weeks with OXA by intraperitoneal injection. Treated WT mice showed all the symptoms of adipose hypotrophy, whereas *Fog2^{Rb-/-Rb-}* mice, which were lean before drug treatment, became fat (Figures 7B–7D). Histological and molecular analysis revealed a concomitant inversion of (1) cell morphological features (Figure 7E; Figure S8); (2) *Ucp1*, *Cidea*, and *Cox5a* expression (Figure 7F); and (3) mitochondrion numbers (Figure 7G). These observations are consistent with the induction of a subcutaneous browning of WAT in WT mice and an inhibition of WAT browning in *Fog2^{Rb-/-Rb-}* mice by OXA. Indeed, we also observed that OXA treatment corrected blood lactate level in *Fog2^{Rb-/-Rb-}* mice, but it led to an increase in blood lactate in WT mice (Figure 7H). *Fog2^{Rb-/-Rb-}* mice compensated for their inability to recycle lactate through a metabolic adaptation involving a switch to BAT. The molecular mechanisms by which OXA modifies the phenotypes of WT and *Fog2^{Rb-/-Rb-}* mice remain to be established.

DISCUSSION

The members of the GATA family of transcription factors (six members in mammals) and their cofactors (FOG-1 and FOG-2) play a key role in tissue-specific development and differentiation. The FOG cofactors bind exclusively to the N-terminal zinc finger of GATA protein, cannot bind DNA, have no independent function, and act together with GATA to control cell differentiation (Chlon and Crispino, 2012). GATA-1/2/3 and FOG-1 are predominantly expressed in hematopoietic cells, whereas the other GATA members and FOG-2 participate in control of the differentiation of most other cell types (Cantor and Orkin, 2005; Patient and McGhee, 2002). We recently discovered a new pathway in which the dynamic regulation of GATA-1/FOG-1 binding is directly connected to the control of cell proliferation by the pRb/E2F pathway. We have demonstrated the functional importance of an LXCXE pRb-binding

site of GATA-1 as a key component of this regulation controlling both erythroid proliferation and differentiation: mutation of this motif abolishes the anti-proliferative function of GATA-1 *in vitro* and leads to the death of mice by anemia *in vivo* (Kadri et al., 2009). We show here that GATA-1 and FOG-2 are the only members of the GATA and FOG families to have an N-terminal LXCXE pRb-binding motif. Unlike GATA-1, which inhibits cell division, FOG-2 promotes proliferation. The mutation of its LXCXE motif prevents this effect, and it has an impact on adipogenesis *in vitro* and *in vivo*.

We previously showed that mutation of the LXCXE pRb-binding site of GATA-1 prevents E2F sequestration within GATA-1/pRb/E2F complexes (Kadri et al., 2009, 2015), resulting in changes to the GATA-1/FOG-1 and pRb/E2F equilibrium. As biochemical analyses of the endogenous FOG-2/pRb/E2F complexes in WT and *Fog2^{Rb-/-Rb-}* mice were inconclusive, it was not possible to directly demonstrate the underlying molecular mechanism involved in the proliferation increase induced by FOG-2. However, loss-of-function data seem to indicate a direct connection between FOG-2 and pRb: (1) *Fog2^{Rb-/-Rb-}* mice display abdominal WAT hypoplasia, (2) *Fog2^{Rb-/-Rb-}* MEFs and preadipocytes display an impairment of proliferation, (3) the expression of several genes involved in cell proliferation and cell cycle progression is misregulated in *Fog2^{Rb-/-Rb-}* MEF cells, and (4) LXCXE mutation of FOG-2 results in a loss of proliferation. Problems evaluating the endogenous physical associations between pRb and LXCXE proteins have repeatedly been reported (Morris and Dyson, 2001). For example, the LXCXE domains of ID-2 (Lasurella et al., 1996) and of the oncoproteins E1A, E7, and SV40 large T antigen (Helt and Galloway, 2003) have clearly been implicated in pRb/E2F regulation, but no evidence of a direct association between these proteins and pRb has ever been reported.

The phenotype of *Fog2^{Rb-/-Rb-}* mice is consistent with a KO of associated factors. For example, GATA-2/3 gene KO enhances adipogenic potential (Tong et al., 2000), and our model suggests that disruption of one component of the complex can affect the relationship between FOG-2 and pRb/E2F. Thus, like *Fog2^{Rb-/-Rb-}* mice, *pRb^{-/-}* (Calo et al., 2010; Dali-Youcef et al., 2007; Hansen et al., 2004) and *E2f1^{-/-}* (Blanchet et al., 2011) KO mice are resistant to obesity. Collectively, our FOG-2 data and published data for pRb, E2F, and GATA proteins seem to indicate that these four components act together in the control of adipogenesis.

In light of our previous findings for GATA-1 (Kadri et al., 2009), we conclude that one member of the GATA/FOG complex is involved in pRb regulation, but that GATA-1 and FOG-2 have opposite effects. GATA-1 binding to pRb/E2F-2 slows down the G1/S cell cycle transition, and mice with a GATA-1^{Rb-} mutant protein are unable to achieve normal erythroid differentiation and die from anemia by E11 (Kadri et al., 2009). Conversely, we show here that mutation of LXCXE pRb-binding motif of FOG-2 reduces adipocyte precursor number (WAT hypoplasia in *Fog2^{Rb-/-Rb-}* mice) and MEF and preadipocyte cell proliferation. These opposite effects of GATA-1 and FOG-2 in the control of cell proliferation are not yet fully understood. Similar results have been observed with other proteins bearing an LXCXE motif,

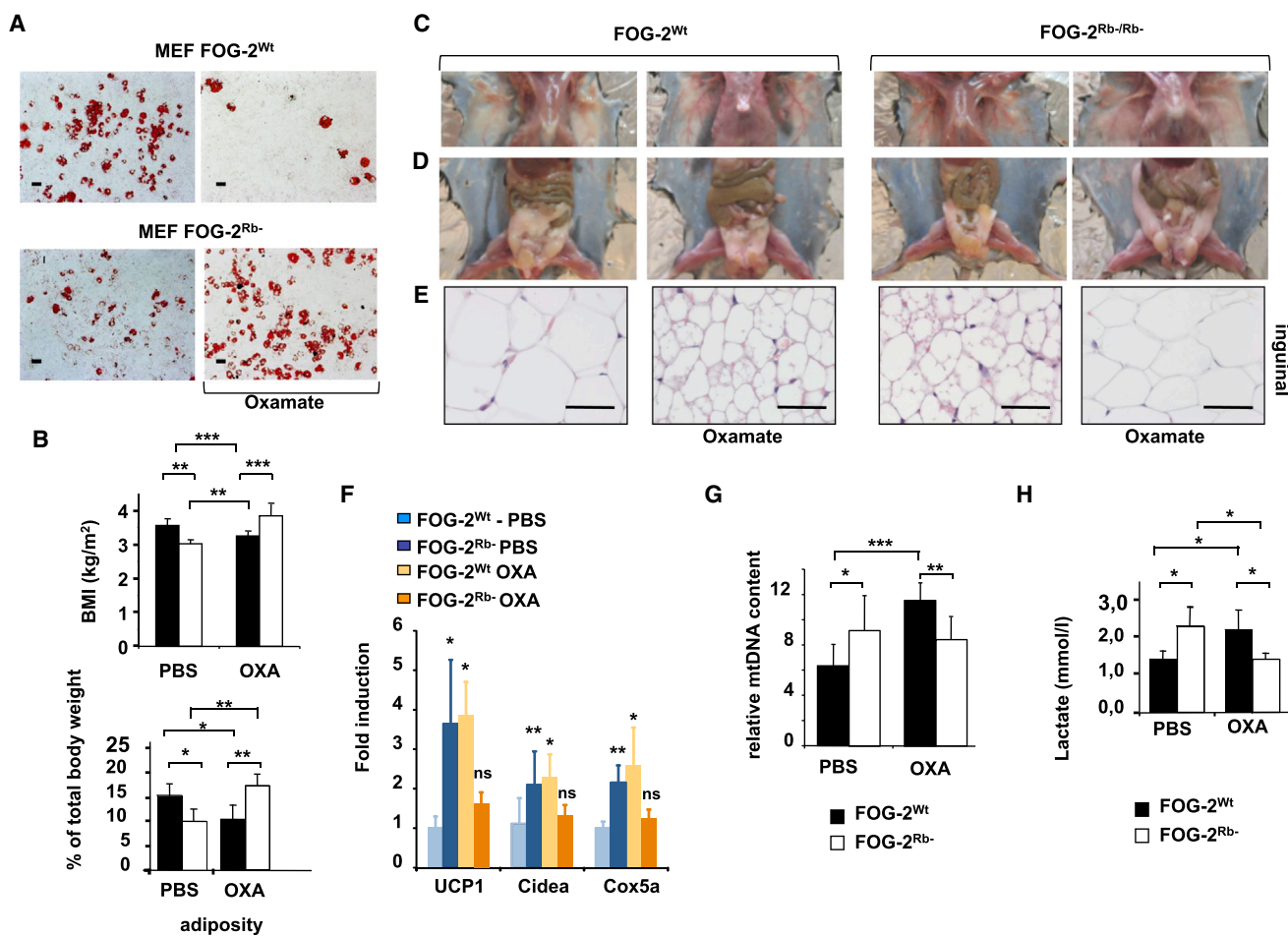


Figure 7. Oxamate Reverses Adiposity of WT and *Fog2^{Rb-Rb-}* Mice *In Vitro* and *In Vivo*

(A) Oil red staining of WT and *Fog2^{Rb-Rb-}* E14.5 MEF cells induced at confluency to differentiate 7 days into adipocytes with or without sodium oxamate (OXA) (three independent experiments give the same result). Scale bar, 50 μ m.

(B) Quantification of adiposity increase of BMI (kg/m²) and adiposity (%) of 10-week-old WT and *Fog2^{Rb-Rb-}* male mice injected daily with PBS or oxamate for 5 weeks (one-tailed Mann-Whitney test, $\alpha = 0.05$; n = 8/group) under a regular diet.

(C and D) Macroscopic comparison of inguinal (C) and abdominal (D) fat of corresponding mice.

(E) Representative H&E staining of inguinal FAT sections from corresponding mice (scale bar, 50 μ m). See also Figure S8.

(F) qRT-PCR relative quantification of genes specifically expressed in BAT (*Ucp1*, *Cidea*, and *Cox5a*) in inguinal FAT of WT and *Fog2^{Rb-Rb-}* mice injected with PBS or oxamate for 5 weeks.

(G) qPCR estimation of mtDNA level with and without oxamate (OXA) treatment in inguinal FAT (for F and G, one-way ANOVA with Bonferroni post test, $\alpha = 0.05$; and n = 5 per group).

(H) Blood lactate level of WT and *Fog2^{Rb-Rb-}* male mice injected with PBS or OXA, (one-tailed Mann-Whitney test, $\alpha = 0.05$; n = 5/group/genotype). See also Figure S6.

Data are mean \pm SD.

such as ID-2 (Lasorella et al., 1996) and the oncoproteins E1A, E7, and SV40 large T antigen (Morris and Dyson, 2001).

The hematopoietic factor GATA-1 is phosphorylated by AKT at Ser310. The non-hematopoietic GATA cofactor FOG-2 also has a Ser residue in position 532 that could be targeted for AKT phosphorylation. In erythroid cells, AKT is activated by erythropoietin, which is required, *in vitro*, for erythroid differentiation (Kadri et al., 2005; Zhao et al., 2006). Mice bearing a mutation Ser310 to be replaced by an alanine residue (Gata-1S310A) suffer from fatal anemia if a compensatory pathway for E2F2 production involving IGF-I signaling is simultaneously abolished.

Thus, signaling via the IGF-I receptor results in physiological adaptations compensating for the abnormal sequestration of E2F2 by the GATA-1S310A/pRb complex (Kadri et al., 2015). We deduce that FOG-2 phosphorylation by AKT may also be involved in the dynamics of this pRb pathway. It is interesting to note that the restriction of erythropoietin receptor expression to hematopoietic tissues promotes obesity (Teng et al., 2011) and erythropoietin overexpression (Hojman et al., 2009) or the loss of AKT (Wan et al., 2012) protects against diet-induced obesity. AKT activation by erythropoietin or other cytokines may induce FOG-2 phosphorylation, increase FOG-2/GATA

binding, and enhance FOG-2/pRb dissociation. The existence of this putative pathway remains to be established *in vivo*: studies of mice with a KI of a mutated gene encoding a FOG-2 protein in which Ser532 is replaced by an alanine residue.

Overall, the data presented here indicate that disruption of the LXCXE pRb-binding site of FOG-2 in adipocyte progenitors may induce WAT browning, providing support for a role of pRb in directing the differentiation of bipotent adipocyte precursors into white or brown adipocytes. This hypothesis is not new, and retinoblastoma protein haploinsufficiency (Mercader et al., 2009; Petrov et al., 2016), disruption (Calo et al., 2010; Dali-Youcef et al., 2007; Hansen et al., 2004), and indirect inhibition (Hu et al., 2015; Scimè et al., 2005; Wang et al., 2013) have identified pRb as a regulator of the commitment of preadipocytes to brown adipogenesis.

Finally, our findings highlight the potential role of lactate in the conversion of WAT to BAT. Lactate is the main by-product of glucose under conditions of anaerobiosis/hypoxia, for example, during exercise. Lactate serves not only as an energy substrate but also as a molecule signaling the fate and function of adipose cells (Cai et al., 2008; Rooney and Trayhurn, 2011). Lactate has been reported to induce UCP-1 expression and, consequently, BAT production. The inhibition of lactate import abolishes this process (Carrière et al., 2014). Lactate upregulation during browning increases Fgf21 expression in WAT adipocytes, contributing to UCP-1 expression (Jeanson et al., 2016). However, extrinsic processes, such as the CNS regulation of food intake and body weight by pyruvate/lactate balance (Lam et al., 2008), may make interpretation difficult. On the other hand, as FOG-2 and GATA-3 are required in brain functions (Lu et al., 1999), an intrinsic control of food intake, body weight, and hyperactivity by FOG-2/pRb could be a possibility. The effects of injecting OXA in WT and *Fog2^{Rb-Rb}* mice highlight the complex interplay among several metabolic pathways regulating pyruvate/lactate homeostasis. OXA, a non-toxic pyruvate analog, inhibits both the A and B isoforms of LDH responsible for controlling pyruvate/lactate interconversion in several metabolic organs, including the muscle, heart, liver, and adipose tissue (Cassady et al., 2001; Wong et al., 1997). LDH-A catabolizes pyruvate to lactate and generates NAD⁺, an essential cofactor for other metabolic enzymes. By contrast, LDH-B converts lactate to pyruvate, making it possible for cells to use lactate as a source of nutrients for oxidative metabolism (muscle and heart), gluconeogenesis (liver), and lipogenesis. The functions of LDH isozymes have probably been underestimated and have yet to be fully elucidated. OXA also targets other enzymes, potentially accounting for its impact on metabolic flux (Morino-Sánchez et al., 2017). OXA has also been identified as a possible inhibitor of members of the MCT pyruvate/lactate transporter family (Halestrap, 2012). It is, therefore, difficult to interpret the effects of OXA injection, leading to an increase in blood lactate level and a decrease in body weight (catabolism) in WT mice and the opposite effect in mutant mice (anabolism). Mutation of the LXCXE motif of FOG-2 in MEF cells leads to a browning of these cells and OXA treatment reverses this process. We can therefore conclude that this pathway is at least partly cell autonomous.

Our data identify FOG-2 as a new switch in lineage commitment and expansion. FOG-2 may be a relevant target in attempts to control the balance between WAT and BAT. Thus, a single member of each component of the GATA/FOG complex, GATA-1 and FOG-2, contains a functional LXCXE pRb-binding motif in an N-terminal position and is involved in pRb/E2F regulation. These both proteins were unexpectedly found to have different roles in the control of red blood cell production and adipocyte production, respectively. These two models shed light on the complex processes involved in the normal and pathological regulation of the crucial balance control between cell proliferation and differentiation within tissues.

EXPERIMENTAL PROCEDURES

MEF Induction of Adipogenesis

For differentiation, MEFs were seeded at 62.5×10^3 cells/well of MW24, and 2-day post-confluent cells (designated day 0) were switched to adipocyte differentiation medium (ADM; AmnioMax C-100 basal medium [Invitrogen] supplemented with 7.5% fetal bovine serum [FBS; 16030, Gibco, Invitrogen], 7.5% AmnioMax-C100 Supplement, 2 mM Glutamine and 1× penicillin/streptomycin and containing 1 μ M dexamethasone [Sigma], 0.5 mM methylisobutylxanthine [I7018, Sigma], 5 μ g/mL insulin [Sigma], and 0.5 μ M rosiglitazone [R2408, Sigma] for 2 days. From day 2, the medium contained only 5 μ g/mL insulin and 0.5 μ M rosiglitazone and was changed every 2 days. Full differentiation was achieved after 6–10 days. For the LDH inhibition experiment, post-confluent MEFs were induced to differentiate in the ADM without rosiglitazone in the presence of 20 mM OXA in PBS 1×, and the medium was changed every 2 days for 7 days.

Cell Cycle Analysis

Cell cycle analysis was performed on asynchronously growing MEFs with a NucleoCounter NC-3000 (Chemometec) instrument. Cells were harvested and stained with 10 μ g/mL DAPI according to the manufacturer's instructions, and DAPI staining intensity was then analyzed as an indicator of DNA content. The DNA content histograms obtained were used to determine the numbers of cells in the various stages of the cell cycle and to plot the cell cycle distribution of MEFs.

Bodipy and MitoTracker Labeling

Bodipy^{493/503} (790389, Sigma, 1 mg/mL) and MitoTracker Red (100 nM, M7512, Molecular Probes) were used for the simultaneous staining of live cells for 30 min at 37°C in culture medium before fixation and staining with Hoechst 33342 (2.5 μ g/mL, Molecular Probes H3570). Fluorescent images were captured with a Leica fluorescence microscope equipped with a Nikon DXM 1200C digital camera.

Oil Red Staining

Dishes were washed with PBS and cells were fixed with Formalin solution 10% (HT5011, Sigma) for 10 min at 20°C. Cells were washed 2 times with H₂O and one time with 60% isopropanol. Cells were dried completely at room temperature and labeled with filtered oil red solution (0.6 g oil red, O0625 Sigma, dissolved in 60% isopropanol) for 10 min. Oil red solution was removed and the cells were washed 4 times with water before the acquisition of images under a microscope.

Animals and Diet

Mice were housed in a temperature-controlled (at 22.5°C \pm 1°C) room on a 12-hr light/dark cycle in an animal facility of CEA FAR. Animals were maintained on a standard chow diet containing 5.1% fat (A03-10, SAFE Diets.com).

Cold Experiment

For the cold challenge experiment, male mice acclimated at 28°C–30°C were placed at 4°C for several hours or progressively acclimated at 4°C for 10 days. 10-week-old WT and *Fog2^{Rb-Rb}* mice were individually housed in cages and

acclimated to cold (2 hr per day) during 3 days and maintained at 6°C during 10 days. Mice were euthanized and studied.

OXA Treatment

Sodium OXA (O2751, Sigma) was dissolved in PBS at 50 mg/mL. Mice received an intraperitoneal injection with 15 mg OXA (300 μ L) or PBS (300 μ L/30 g body weight [BW]) every 24 hr for 5 weeks. This treatment was done under a regular diet.

Metabolic Experiments

Glucose levels in blood from tail were measured, on conscious mice after a 16-hr fast, with test strips on a glucometer (Roche, Accucheck Performa nano). In the same condition, lactate levels were measured with test strips on an EKF Diagnostics lactate meter (Lactate Scout). For plasma analysis, blood was collected from retro-orbital sinus after overnight fasting. Blood was kept on ice until centrifugation (1,500 \times g, 15 min at 4°C), and the plasma was stored at -20°C until analysis. Plasma mouse adipokines were measured using Multiplex Biomarkers Immunoassays for Luminex xMAP technology (MMHMAG-44K, Millipore, France).

Glucose, Insulin, Pyruvate, and Lactate Tolerance Tests

Tolerance tests were performed by fasting the mice overnight for 6 or 16 hr and then injecting glucose (D-Glucose G8769, Sigma, 1 g kg⁻¹), insulin (I2643, Sigma, 0.75 g kg⁻¹), pyruvate (P4562, Sigma, 2 g kg⁻¹), or lactate (L7022, Sigma, 1.5 g kg⁻¹) intraperitoneally. Blood samples were collected from tail, and glucose and lactate level measurements were performed at specific time points, indicated as described in [Metabolic Experiments](#).

Statistical Analyses

Values are expressed as mean \pm SD or mean \pm SEM when precised. Data determined to be normally distributed as the maximum and the minimum values in each dataset were <3 SD from the mean. Data were analyzed using Prism 6.0 (GraphPad Software) by one-tailed Student's t test or one-way ANOVA with Bonferroni post-test ($\alpha < 0.05$). Parameters measured over multiple time points were analyzed with two-way ANOVA with Bonferroni post-test; time was a within-subject factor. Otherwise, as specified in the legend, when *F*-test indicated statistically different variance ($\alpha < 0.05$), the unpaired one-tailed Mann-Whitney test was used ($\alpha < 0.05$). The significance levels displayed in figures are as follows: * $p < 0.05$, ** $p < 0.01$, *** $p < 0.001$, and "NS" means no significance. There was no blinding, and no particular randomization method was used to assign individuals to experimental groups. Sample or experiment sizes were determined empirically to achieve sufficient statistical power.

DATA AND SOFTWARE AVAILABILITY

The accession number for the proliferating WT and *Fog2*^{Rb-/-Rb-} E14.5 MEF cells microarray data reported in this paper is GEO: GSE90859.

SUPPLEMENTAL INFORMATION

Supplemental Information includes Supplemental Experimental Procedures and eight figures and can be found with this article online at <https://doi.org/10.1016/j.celrep.2017.11.098>.

ACKNOWLEDGMENTS

We thank A. Langele for technical assistance, A. Schmitt and J.M. Masse (Cochin Imaging Facility, Paris, France) for electron microscopy analysis, S. Luccantoni (CEA, Fontenay aux Roses, France) for paraffin sections of mouse intestine, and T. Kortulewski (CEA, Fontenay aux Roses, France) for assistance with Cell Profiler pipelines. We acknowledge the technical platform metabolism of the Unit "Biologie Fonctionnelle et Adaptative" for metabolic analysis. This work was supported by grants from ANR (Chaires d'excellence and industrielle awarded to P.L. and S.C.). KI mice were generated at the Mouse Clinical Institute (Illkirch, France) 801 and supported by the GIS Institut

des Maladies Rares (IR 1673 to S.C.). T.P. was supported by the Egid/ SIAM2011 Franco-Thai Program and a CEA fellowship, and O.G. was supported by a fellowship from ANR.

AUTHOR CONTRIBUTIONS

O.G. designed, performed the experiments, and made intellectual contributions to the work. M.G.-L., R.D., Z.K., and T.P. performed the experiments. C.B. performed and interpreted the histological studies. S.C., O.G., L.M.-C., S.L., S.F., and Z.K. analyzed the data. S.C., originator of the central hypothesis, conceived and supervised this study. S.C. and P.L. wrote the paper.

DECLARATION OF INTERESTS

The authors declare no competing interests.

Received: June 1, 2017

Revised: October 12, 2017

Accepted: November 28, 2017

Published: December 19, 2017

REFERENCES

- Aguilar, V., and Fajas, L. (2010). Cycling through metabolism. *EMBO Mol. Med.* 2, 338–348.
- Blanchet, E., Annicotte, J.S., Lagarrigue, S., Aguilar, V., Clapé, C., Chavey, C., Fritz, V., Casas, F., Apparailly, F., Auwerx, J., and Fajas, L. (2011). E2F transcription factor-1 regulates oxidative metabolism. *Nat. Cell Biol.* 13, 1146–1152.
- Cai, T.-Q., Ren, N., Jin, L., Cheng, K., Kash, S., Chen, R., Wright, S.D., Taggart, A.K.P., and Waters, M.G. (2008). Role of GPR81 in lactate-mediated reduction of adipose lipolysis. *Biochem. Biophys. Res. Commun.* 377, 987–991.
- Calo, E., Quintero-Estades, J.A., Danielian, P.S., Nedelcu, S., Berman, S.D., and Lees, J.A. (2010). Rb regulates fate choice and lineage commitment in vivo. *Nature* 466, 1110–1114.
- Cantor, A.B., and Orkin, S.H. (2002). Transcriptional regulation of erythropoiesis: an affair involving multiple partners. *Oncogene* 21, 3368–3376.
- Cantor, A.B., and Orkin, S.H. (2005). Coregulation of GATA factors by the Friend of GATA (FOG) family of multitype zinc finger proteins. *Semin. Cell Dev. Biol.* 16, 117–128.
- Carrière, A., Jeanson, Y., Berger-Müller, S., André, M., Chenouard, V., Arnaud, E., Barreau, C., Walther, R., Galinier, A., Wdziekonski, B., et al. (2014). Browning of white adipose cells by intermediate metabolites: an adaptive mechanism to alleviate redox pressure. *Diabetes* 63, 3253–3265.
- Cassady, C.J., Phillis, J.W., and O'Regan, M.H. (2001). Further studies on the effects of topical lactate on amino acid efflux from the ischemic rat cortex. *Brain Res.* 901, 30–37.
- Chlon, T.M., and Crispino, J.D. (2012). Combinatorial regulation of tissue specification by GATA and FOG factors. *Development* 139, 3905–3916.
- Dali-Youcef, N., Matak, C., Coste, A., Messaddeq, N., Giroud, S., Blanc, S., Koehl, C., Champy, M.F., Chambon, P., Fajas, L., et al. (2007). Adipose tissue-specific inactivation of the retinoblastoma protein protects against diabetes because of increased energy expenditure. *Proc. Natl. Acad. Sci. USA* 104, 10703–10708.
- Giovannetti, E., Wang, Q., Avan, A., Funel, N., Lagerweij, T., Lee, J.-H., Caretti, V., van der Velde, A., Boggi, U., Wang, Y., et al. (2014). Role of CYB5A in pancreatic cancer prognosis and autophagy modulation. *J. Natl. Cancer Inst.* 106, djt346.
- Guan, W., Cheng, F., Wu, H., Cao, Q., Zhu, X., Fan, Y., Zhu, H., and Zhou, Y. (2017). GATA binding protein 3 is correlated with leptin regulation of PPAR γ 1 in hepatic stellate cells. *J. Cell. Mol. Med.* 21, 568–578.
- Halestrap, A.P. (2012). The monocarboxylate transporter family—Structure and functional characterization. *IUBMB Life* 64, 1–9.

- Hansen, J.B., Jørgensen, C., Petersen, R.K., Hallenborg, P., De Matteis, R., Boye, H.A., Petrovic, N., Enerbäck, S., Nedergaard, J., Cinti, S., et al. (2004). Retinoblastoma protein functions as a molecular switch determining white versus brown adipocyte differentiation. *Proc. Natl. Acad. Sci. USA* *101*, 4112–4117.
- Helt, A.M., and Galloway, D.A. (2003). Mechanisms by which DNA tumor virus oncoproteins target the Rb family of pocket proteins. *Carcinogenesis* *24*, 159–169.
- Hojman, P., Brolin, C., Gissel, H., Brandt, C., Zerahn, B., Pedersen, B.K., and Gehl, J. (2009). Erythropoietin over-expression protects against diet-induced obesity in mice through increased fat oxidation in muscles. *PLoS ONE* *4*, e5894.
- Hu, X., Luo, P., Peng, X., Song, T., Zhou, Y., Wei, H., Peng, J., and Jiang, S. (2015). Molecular cloning, expression pattern analysis of porcine Rb1 gene and its regulatory roles during primary dedifferentiated fat cells adipogenic differentiation. *Gen. Comp. Endocrinol.* *214*, 77–86.
- Jack, B.H., and Crossley, M. (2010). GATA proteins work together with friend of GATA (FOG) and C-terminal binding protein (CTBP) co-regulators to control adipogenesis. *J. Biol. Chem.* *285*, 32405–32414.
- Jeanson, Y., Ribas, F., Galinier, A., Arnaud, E., Ducos, M., André, M., Chenouard, V., Villarroja, F., Casteilla, L., and Carrière, A. (2016). Lactate induces FGF21 expression in adipocytes through a p38-MAPK pathway. *Biochem. J.* *473*, 685–692.
- Kadri, Z., Maouche-Chretien, L., Rooke, H.M., Orkin, S.H., Romeo, P.H., Mayeux, P., Leboulch, P., and Chretien, S. (2005). Phosphatidylinositol 3-kinase/Akt induced by erythropoietin renders the erythroid differentiation factor GATA-1 competent for TIMP-1 gene transactivation. *Mol. Cell. Biol.* *25*, 7412–7422.
- Kadri, Z., Shimizu, R., Ohneda, O., Maouche-Chretien, L., Gisselbrecht, S., Yamamoto, M., Romeo, P.H., Leboulch, P., and Chretien, S. (2009). Direct binding of pRb/E2F-2 to GATA-1 regulates maturation and terminal cell division during erythropoiesis. *PLoS Biol.* *7*, e1000123.
- Kadri, Z., Lefevre, C., Goupille, O., Penglong, T., Granger-Locatelli, M., Fucharoen, S., Maouche-Chretien, L., Leboulch, P., and Chretien, S. (2015). Erythropoietin and IGF-1 signaling synchronize cell proliferation and maturation during erythropoiesis. *Genes Dev.* *29*, 2603–2616.
- Lam, C.K.L., Chari, M., Wang, P.Y.T., and Lam, T.K.T. (2008). Central lactate metabolism regulates food intake. *Am. J. Physiol. Endocrinol. Metab.* *295*, E491–E496.
- Lasorella, A., Iavarone, A., and Israel, M.A. (1996). Id2 specifically alters regulation of the cell cycle by tumor suppressor proteins. *Mol. Cell. Biol.* *16*, 2570–2578.
- Lu, J.R., McKinsey, T.A., Xu, H., Wang, D.Z., Richardson, J.A., and Olson, E.N. (1999). FOG-2, a heart- and brain-enriched cofactor for GATA transcription factors. *Mol. Cell. Biol.* *19*, 4495–4502.
- Mercader, J., Ribot, J., Murano, I., Feddersen, S., Cinti, S., Madsen, L., Kristiansen, K., Bonet, M.L., and Palou, A. (2009). Haploinsufficiency of the retinoblastoma protein gene reduces diet-induced obesity, insulin resistance, and hepatosteatosis in mice. *Am. J. Physiol. Endocrinol. Metab.* *297*, E184–E193.
- Mo, S.-J., Liu, X., Hao, X.-Y., Chen, W., Zhang, K.-S., Cai, J.-P., Lai, J.-M., Liang, L.-J., and Yin, X.-Y. (2016). EYA4 functions as tumor suppressor gene and prognostic marker in pancreatic ductal adenocarcinoma through β -catenin/ID2 pathway. *Cancer Lett.* *380*, 403–412.
- Moreno-Sánchez, R., Marín-Hernández, Á., Del Mazo-Monsalvo, I., Saavedra, E., and Rodríguez-Enríquez, S. (2017). Assessment of the low inhibitory specificity of oxamate, aminooxyacetate and dichloroacetate on cancer energy metabolism. *Biochim. Biophys. Acta* *1861* (1 Pt A), 3221–3236.
- Morris, E.J., and Dyson, N.J. (2001). Retinoblastoma protein partners. *Adv. Cancer Res.* *82*, 1–54.
- Ohtani, K., Iwanaga, R., Nakamura, M., Ikeda, M., Yabuta, N., Tsuruga, H., and Nojima, H. (1999). Cell growth-regulated expression of mammalian MCM5 and MCM6 genes mediated by the transcription factor E2F. *Oncogene* *18*, 2299–2309.
- Patient, R.K., and McGhee, J.D. (2002). The GATA family (vertebrates and invertebrates). *Curr. Opin. Genet. Dev.* *12*, 416–422.
- Petrov, P.D., Palou, A., Bonet, M.L., and Ribot, J. (2016). Cell-Autonomous Brown-Like Adipogenesis of Preadipocytes From Retinoblastoma Haploinsufficient Mice. *J. Cell. Physiol.* *231*, 1941–1952.
- Rooney, K., and Trayhurn, P. (2011). Lactate and the GPR81 receptor in metabolic regulation: implications for adipose tissue function and fatty acid utilisation by muscle during exercise. *Br. J. Nutr.* *106*, 1310–1316.
- Rylski, M., Welch, J.J., Chen, Y.Y., Letting, D.L., Diehl, J.A., Chodosh, L.A., Blobel, G.A., and Weiss, M.J. (2003). GATA-1-mediated proliferation arrest during erythroid maturation. *Mol. Cell. Biol.* *23*, 5031–5042.
- Scimè, A., Grenier, G., Huh, M.S., Gillespie, M.A., Bevilacqua, L., Harper, M.-E., and Rudnicki, M.A. (2005). Rb and p107 regulate preadipocyte differentiation into white versus brown fat through repression of PGC-1 α . *Cell Metab.* *2*, 283–295.
- Shalizi, A., Gaudillière, B., Yuan, Z., Stegmüller, J., Shirogane, T., Ge, Q., Tan, Y., Schulman, B., Harper, J.W., and Bonni, A. (2006). A calcium-regulated MEF2 sumoylation switch controls postsynaptic differentiation. *Science* *311*, 1012–1017.
- Suh, J.M., Gao, X., McKay, J., McKay, R., Salo, Z., and Graff, J.M. (2006). Hedgehog signaling plays a conserved role in inhibiting fat formation. *Cell Metab.* *3*, 25–34.
- Teng, R., Gavrilova, O., Suzuki, N., Chanturiya, T., Schimel, D., Hugendubler, L., Mammen, S., Yver, D.R., Cushman, S.W., Mueller, E., et al. (2011). Disrupted erythropoietin signalling promotes obesity and alters hypothalamus pro-opiomelanocortin production. *Nat. Commun.* *2*, 520.
- Tevosian, S.G., Deconinck, A.E., Cantor, A.B., Rieff, H.I., Fujiwara, Y., Corfas, G., and Orkin, S.H. (1999). FOG-2: A novel GATA-family cofactor related to multitype zinc-finger proteins Friend of GATA-1 and U-shaped. *Proc. Natl. Acad. Sci. USA* *96*, 950–955.
- Tong, Q., Dalgin, G., Xu, H., Ting, C.N., Leiden, J.M., and Hotamisligil, G.S. (2000). Function of GATA transcription factors in preadipocyte-adipocyte transition. *Science* *290*, 134–138.
- Tsai, J., Tong, Q., Tan, G., Chang, A.N., Orkin, S.H., and Hotamisligil, G.S. (2005). The transcription factor GATA2 regulates differentiation of brown adipocytes. *EMBO Rep.* *6*, 879–884.
- Vergnes, L., and Reue, K. (2014). Adaptive thermogenesis in white adipose tissue: is lactate the new brown(in)g? *Diabetes* *63*, 3175–3176.
- Wan, M., Easton, R.M., Gleason, C.E., Monks, B.R., Ueki, K., Kahn, C.R., and Birnbaum, M.J. (2012). Loss of Akt1 in mice increases energy expenditure and protects against diet-induced obesity. *Mol. Cell. Biol.* *32*, 96–106.
- Wang, J., Liu, R., Wang, F., Hong, J., Li, X., Chen, M., Ke, Y., Zhang, X., Ma, Q., Wang, R., et al. (2013). Ablation of LGR4 promotes energy expenditure by driving white-to-brown fat switch. *Nat. Cell Biol.* *15*, 1455–1463.
- Wong, C., Rodríguez-Pérez, L., Noguera, B., Pérez, A., and Baeza, I. (1997). Selective inhibition of the sperm-specific lactate dehydrogenase isozyme-C4 by N-isopropyl oxamate. *Biochim. Biophys. Acta* *1343*, 16–22.
- Xu, Z., Yu, S., Hsu, C.-H., Eguchi, J., and Rosen, E.D. (2008). The orphan nuclear receptor chicken ovalbumin upstream promoter-transcription factor II is a critical regulator of adipogenesis. *Proc. Natl. Acad. Sci. USA* *105*, 2421–2426.
- Yang, Y., Wu, J., Cai, J., He, Z., Yuan, J., Zhu, X., Li, Y., Li, M., and Guan, H. (2015). PSAT1 regulates cyclin D1 degradation and sustains proliferation of non-small cell lung cancer cells. *Int. J. Cancer* *136*, E39–E50.
- Zeisberg, E.M., Ma, Q., Juraszek, A.L., Moses, K., Schwartz, R.J., Izumo, S., and Pu, W.T. (2005). Morphogenesis of the right ventricle requires myocardial expression of Gata4. *J. Clin. Invest.* *115*, 1522–1531.
- Zhao, W., Kitidis, C., Fleming, M.D., Lodish, H.F., and Ghaffari, S. (2006). Erythropoietin stimulates phosphorylation and activation of GATA-1 via the PI3-kinase/AKT signaling pathway. *Blood* *107*, 907–915.